universität wien

BACHELORARBEIT / BACHELOR THESIS

Titel der Bachelorarbeit / Title of the Bachelor Thesis

„Scattering of Scalar Waves on a Schwarzschild Black Hole“

verfasst von / submitted by

Ludwig Wolfgruber

angestrebter akademischer Grad / in partial fulfilment of the requirements for the degree of

Bachelor of Science

Wien, 2020 / Vienna, 2020

Studienkennzahl lt. Studienblatt / degree programme code as it appears on the student record sheet:	A 676
Studienrichtung lt. Studienblatt / degree programme as it appears on the student record sheet:	Bachelor Physik
Betreut von / Supervisor:	Dr. Maciej Maliborski

Contents

Abstract

Gravitational waves have been an important topic in gravitational and astrophysics for many decades now. In the recent years, due to effective operation of gravitational wave detectors, a new spot shines on this subject. In this Bachelor Thesis we want to compare different approaches on solving the wave equation on a Schwarzschild spacetime with a focus on the obtained quasi normal modes which are a powerful set of parameters which uniquely characterize a black hole.

Gravitationswellen sind seit einigen Jahrzenten ein wichtiges Thema in der Gravitations- und Astrophysik. In den letzten Jahren ist, durch den erfolgreichen Betrieb von Gravitationswellendetektoren, das Thema erneut in den Mittelpunkt gerückt. In dieser Bachelorarbeit werden verschiedene Methoden verglichen, die Wellengleichung in einer Schwarzschild-Raumzeit zu lösen, wobei der Fokus auf den damit gewonnenen quasi-normalen Moden liegt, einem äusserst aussagekräftigen Menge an Parametern, die ein schwarzes Loch eindeutig charakerisieren.

1 Introduction

1.1 The Wave Equation in General Relativity

The Einstein Equations are a set of non-linear partial differential equations, which build the core of General Relativity (GR). Put in a nutshell, they tell how spacetime influences the behavior of matter and how matter influences the evolution of spacetime.

The Einstein equations allow waves, so-called gravitational waves, to propagate on the spacetime itself, stretching and compressing it temporarily. Since the non-linearity of these equations makes solving the wave equation exactly impossible, here scalar waves on a fixed black hole as an approximate solution are beeing concerned with.

To study the behavior of scalar waves on a specific spacetime we want to solve the scalar wave equation

$$\Box\Phi = 0 \tag{1}$$

where $\Box = \Box_{g^{\mu\nu}} = g^{\mu\nu}\partial_\mu\partial_\nu$ is the generalized wave operator[1] for a metric $g_{\mu\nu}$ and $\Phi = \Phi(t, r, \vartheta, \varphi)$ is a scalar function of time and three dimensional space, here represented with spherical coordinates. A metric shapes the behaviour of such an operator in two ways. First it defines a bilinear form, the first fundamental form on the spacetime. It tells us how the product $A^\kappa B_\kappa = g_{\kappa\lambda}A^\kappa B^\lambda$ of two vectors A^κ and B^λ is computed in general. This is needed for the evaluation of $\partial^\mu\partial_\nu$ in equation (1) in particular.

[1] In this thesis ∂_μ will be the derivative with respect to the μ^{th} coordinate. Also we will use the Einstein summation convention, where one sums over two repeated indices, if one is a lower and the other one is a upper index, i.e. $\nabla A = \sum_\mu \frac{\partial A^\mu}{\partial x^\mu} = \partial_\mu A^\mu$ for a vector A^μ in Euclidean space.

The second way a metric forms the differential operator from equation (1) is due to the curvature of the spacetime it describes. As shown in [9] differentiation on a curved spacetime is a generalization of differentiation on a flat manifold.

The metric $g_{\mu\nu}$ affects the behavior of equation (1), since it includes off-diagonal terms in comparison to the non relativistic wave operator $\Box = -\partial_t + \sum_{i=1}^{n} \partial_{x_i}$ which is induced by the flat Minkowski metric $\eta_{\mu\nu}$.

In [9] equation (1) generalizes to

$$\frac{1}{\sqrt{g}} \partial_\mu \left(\sqrt{g}\ g^{\mu\nu} \partial_\nu \Phi \right) = 0 \tag{2}$$

where $g = \det g_{\mu\nu}$.

1.2 The Schwarzschild Metric

A metric $g_{\mu\nu}$ can be a solution to the Einstein Equations. A metric can be represented by a symmetric matrix $(g_{\mu\nu})$, or by an infinitesimal line element $\mathrm{d}s^2$:

$$\mathrm{d}s^2 = g_{\mu\nu} \mathrm{d}x^\mu \mathrm{d}x^\nu \ . \tag{3}$$

The metric holds, together with a manifold, all the information necessary to describe a particular spacetime.

The metric for a flat spacetime in Cartesian coordinates is the Minkowski metric $\eta_{\mu\nu}$ which can be represented by the matrix

$$(\eta_{\mu\nu}) = \mathrm{diag}(-1, 1, 1, 1) \ . \tag{4}$$

Note that in this thesis the units for the speed of light c and the gravitational constant G will be equal to one if not stated elsewise. The representation as an infinitesimal line element works out to be

$$\mathrm{d}s^2 = \eta_{\mu\nu} \mathrm{d}x^\mu \mathrm{d}x^\nu = -\mathrm{d}t^2 + \mathrm{d}x^2 + \mathrm{d}y^2 + \mathrm{d}z^2 \tag{5}$$

or in spherical coordinates

$$\begin{aligned} \mathrm{d}s^2 &= -\mathrm{d}t^2 + \mathrm{d}r^2 + r^2\ \mathrm{d}\vartheta^2 + r^2 \sin^2\vartheta\ \mathrm{d}\varphi^2 \\ &= \mathrm{d}t^2 + \mathrm{d}r^2 + r^2\ \mathrm{d}\hat{\sigma}^2. \end{aligned} \tag{6}$$

Here $\hat{\sigma}^2$ is the metric of the unit sphere in three dimensions: $\hat{\sigma}^2 = \mathrm{d}\vartheta^2 + \sin^2\vartheta\ \mathrm{d}\varphi^2$. It can be seen that the generalized wave equation (2) simplifies to the common wave equation (1) if $g_{\mu\nu}$ is the Minkowski metric $\eta_{\mu\nu}$.

The Schwarzschild metric or Schwarzschild solution is the simplest analytical, non-trivial solution to the Einstein equations. It is the solution for a spacetime with one single resting mass M, which turns out to be a static, spherically symmetric metric. Since we want to study waves on such a Schwarzschild spacetime, $g_{\mu\nu}$ will from now on denote the Schwarzschild metric which is given as

$$\mathrm{d}s^2 = -\left(1 - \frac{2m}{r}\right)\ \mathrm{d}t^2 + \left(1 - \frac{2m}{r}\right)^{-1}\ \mathrm{d}r^2 + r^2\ \mathrm{d}\vartheta^2 + r^2\ \mathrm{d}\hat{\sigma}^2. \tag{7}$$

The m above is defined as $m = \frac{GM}{c^2}$ which implies that in units where $G = c = 1$, it follows that $m = M$. As one can easily see, the Schwarzschild metric (7) converges to the Minkowski metric (6) for m going to zero. Since equation (7) is a full description of a Schwarzschild black hole, such an object is fully determined by only one parameter[2]: its mass M.

1.2.1 Eddington-Finkelstein Coordiantates

By taking a closer look at the Schwarzschild metric from equation (7) one realizes that it becomes singular for two values of r: at the point $r = 0$ and at $r = 2m$, the later one being called the Schwarzschild, or event horizon. While the singularity at $r = 0$ is intrinsic to a black hole, the event horizon is a coordinate singularity and can be removed by a suitable coordinate transformation.

A first step to perform such a transformation is the definition of the tortoise coordinate r_*:

$$r_* = r + 2m \ln\left(\frac{r}{2m} - 1\right) \tag{8}$$

It spans the whole real number line with $r_* \to -\infty$ for $r \to 2m$ and $r_* \to \infty$ for $r \to \infty$. With this coordinate one can also define a fitting t_*:

$$t_* = t + r_* - r = t + 2m \ln\left(\frac{r}{2m} - 1\right) \tag{9}$$

The coordinates $(t_*, r, \vartheta, \varphi)$ are called the Eddington-Finkelstein coordinates. Expressed in those coordinates, the Schwarzschild metric looks like

$$\mathrm{d}s^2 = -\left(1 - \frac{2m}{r}\right)\, \mathrm{d}t_*^2 + \frac{4m}{r}\, \mathrm{d}t_*\, \mathrm{d}r + \left(1 + \frac{2m}{r}\right)\, \mathrm{d}r^2 + r^2\, \mathrm{d}\hat{\sigma}^2. \tag{10}$$

Notice how the first term vanishes at $r = 2m$, but there is no singularity apart from the one at $r = 0$ left.

1.2.2 Constant Mean Curvature

As the author of [13] mentions it is physically relevant to look at gravitational radiation signals, as they can be detected with gravitational wave detectors, at *null infinity*.

To do this the author proposes the conformal method introduced by Penrose, where a rescaling $\tilde{g} = \Omega^2 g$ of the physical metric g by some scalar factor Ω implies a transformation to a wave equation $\Box\Phi = 0$ which can be written as $\left(\Box - \frac{1}{6}R\right)\Phi = 0$ because the Ricci scalar R vanishes for the Schwarzschild solution of a black hole [6, 11]. The transformation works out to be

$$\left(\tilde{\Box} - \frac{1}{6}\tilde{R}\right)\tilde{\Phi} = \left(\Box - \frac{1}{6}R\right)\Phi\ , \quad \text{with } \tilde{\Phi} = \frac{\Phi}{\Omega}\ , \quad \Omega > 0. \tag{11}$$

[2]Descriptions for more complex black holes also depend on other parameters, e.g. their angular momentum and their charge, see [7].

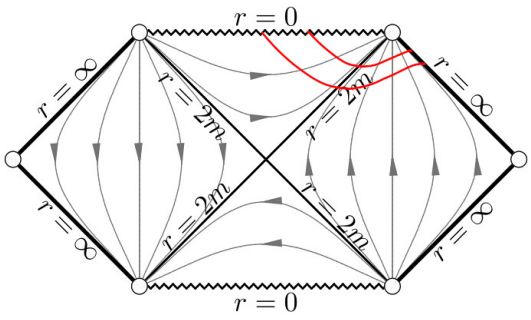

Figure 1: Conformal diagram of a Schwarzschild metric. The red curves are scetched examples for constant mean curvature.

The wave equation with respect to the rescaled metric becomes $\tilde{\Box}\tilde{\Phi} - \tilde{R}/6 = 0$. $\tilde{R}$ is the Ricci scalar of the $\tilde{g}$ respectively.

In [13] the class of spherically symmetric constant mean curvature (CMC) foliations of Schwarzschild spacetime are presented as convenient foliations covering the region from the Schwarzschild radius to *null infinity*. A transformation from common Schwarzschild coordinates to the time coordinate of a CMC foliation can be written as

$$\tilde{t} = t - h(r) \tag{12}$$

with t and r as the standard Schwarzschild time and radial coordinate $h(r)$ is the so called height function, whose derivative is given by

$$h'(r) = \frac{\frac{Kr^3}{3} - C}{\left(1 - \frac{2m}{r}\right) P(r)} \ , \tag{13}$$

with

$$P(r) = \sqrt{\left(\frac{Kr^3}{3} - C\right)^2 + \left(1 - \frac{2m}{r}\right) r^4}. \tag{14}$$

The parameters of the foliation are the mean extrinsic curvature K and a constant of integration C. The parameters are chosen in a way that the surfaces of the foliation coming from future *null infinity* run into the future singularity. Such surfaces can be seen in figure 1. The author of [13] suggests the values $K = 0.5$ and $C = 1$, which we follow in this thesis.

The Schwarzschild metric (7) in a CMC foliation can be written as

$$\mathrm{d}s^2 = -\left(1 - \frac{2m\Omega}{\tilde{r}}\right)\Omega^2\,\mathrm{d}\tilde{t}^2 - \frac{2(K\tilde{r}^3/3 - C\Omega^3)}{\tilde{P}(\tilde{r})}\,\mathrm{d}\tilde{t}\,\mathrm{d}\tilde{r} + \frac{\tilde{r}^4}{\tilde{P}^2(\tilde{r})}\,\mathrm{d}\tilde{r}^2 + \tilde{r}^2\,\mathrm{d}\hat{\sigma}^2 \tag{15}$$

with

$$\tilde{P}(\tilde{r}) = \sqrt{\left(\frac{K\tilde{r}^3}{3} - C\Omega^3\right)^2 + \left(1 - \frac{2m(1-\tilde{r}}{\tilde{r}}\right)\Omega^2\tilde{r}^4} \tag{16}$$

and $\Omega = 1 - \tilde{r}$. The compactifying coordinate $\tilde{r}$ is related to the standard Schwarzschild radial coordinate r via

$$r = \frac{\tilde{r}}{1 - \tilde{r}} = \frac{\tilde{r}}{\Omega}. \tag{17}$$

1.3 Quasi Normal Modes

Any conservative many-particle system with an analytic potential can be described around a stable resting position with its normal coordinates $\{\xi_n\}_{n\geq 0}$ [2]. Normal coordinates express the behaviour of a system by means of its natural oscillations. If one expands the potential in those coordinates in a Taylor series around the equilibrium, truncates it after the second order term, one gets a harmonic equation of motion in normal coordinates for small deviations around the resting position. The system then evolves in time, expressed in normal coordinates, as a superposition of

$$\xi_n(t) = A_n \ \mathrm{Re}\Big[e^{i(\omega_n t + \delta_n)}\Big] = A_n \cos(\omega_n t + \delta_n) \ , \tag{18}$$

which are called *normal modes*. The parameters A_n and δ_n are integration constants and describe the amplitude and the offset of the oscillations. The $\omega_n \in \mathbb{R}$ is the natural frequency of the normal mode ξ_n, which is a characteristic for the properties of the system and the potential. The lowest frequency ω_0 is called the basic or fundamental frequency, the higher frequencies are the overtones.

If a system is not conservative it loses energy and performs damped oscillations. This can be described in the sense of normal modes by giving it a complex normal frequency $\omega_n = \omega_{n,\mathrm{re}} + i\omega_{n,\mathrm{im}}$, for ω_{re}, $\omega_{\mathrm{im}} \in \mathbb{R}^+$.[3] It then can be described by

$$\chi_n(t) = A_n \ \mathrm{Re}\Big[e^{i(\omega_n t + \delta_n)}\Big] = A_n \cos(\omega_{n,\mathrm{re}} t + \delta_n) \ e^{-\omega_{n,\mathrm{im}} t + \delta_n} \tag{19}$$

as it is derived and shown in [7]. For a full description of a system such oscillations – the so called *quasi normal modes* (QNM) – are superposed.

In the representation from the previous sections a black hole is always at rest in its equilibrium state. A perturbed black hole is in some exited state, because its reactions with energy and matter around it in whatever form stimulate it. It also dissipates energy away in the form of gravitational waves. Because of those two properties, the small excitement around its equilibrium and the dissipation of energy, the perturbations of a black hole can be described in the form of quasi normal modes.

If a Schwarzschild black hole is exited by some signal, for example a Gaussian wave package, it reacts in three stages: At first it moves according to the stimulating signal and swings itself into its quasi normal modes. In the second

[3] In the literature the sign of the imaginary part of a quasi normal frequency is not specified consistently. In this thesis we will stick to the convention of a positive sign. Cited formulas with a different convention are therefore adjusted.

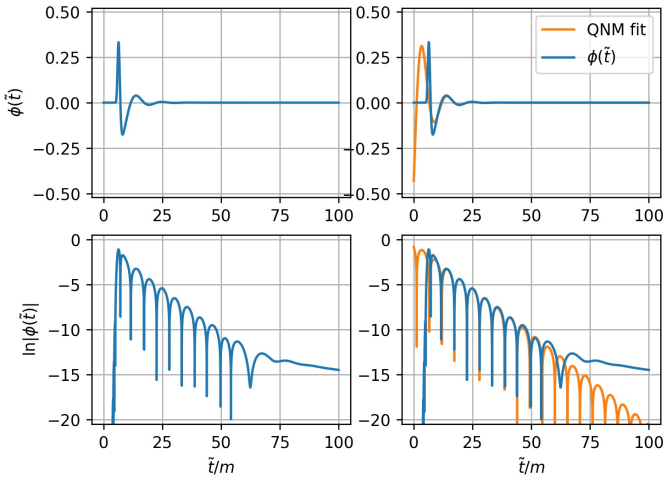

Figure 2: Quasi normal mode with a fit according to equation (19). One can see the characteristic ringdown clearly in the logarithmic presentation between roughly $t = 15$ and $t = 50$. The fit is only applied in this region. From $t = 70$ until the end at $t = 10$ the power-law tail dominates.

part the oscillation in those modes dominate and it rings down according to the damping $\omega_{n,\mathrm{im}}$. In the third phase a power-law fall-off of the form $t^{-\kappa}$, $\kappa > 0$ dominates [7]. In figure 2 such a process and a fitted QNM are shown.

As mentioned above, black holes are fully determined by only a few parameters, a Schwarzschild black hole even by just its mass M. The interesting part about describing a black hole with quasi normal modes is that since the frequencies of these modes contain information about their system, there is a direct connection between the mass of a black hole and its quasi normal modes. In fact in [7] the authors summarize earlier work and present the quasi normal frequencies ω_n as inversely proportional to the mass. They also give an approximation for the quasi normal frequencies which is valid for large values of ℓ:

$$3\sqrt{3}M\omega_n \approx \left(\ell + \frac{1}{2}\right) + i\left(n + \frac{1}{2}\right) \tag{20}$$

Here ℓ arises from a decomposition in spherical harmonics, which will be covered in section 2.1.1. As the imaginary part, which identifies as the damping of the quasi normal frequency grows linearly with n, in a superposition $\sum_{n=0}^{\infty} \chi_n$ the fundamental frequency, which thus has the smallest dumping, will dominate the decay.

Since overtones ($n > 0$) of quasi normal modes of a Schwarzschild black hole decay faster – proportional to e^{-nt} according to equation (20) – and will therefore not be easy to detect in a signal like the one in figure 2, we are going to

focus only on the fundamental modes ω_0 for different ℓ-s. Thus we are changing notation and replace the subscript of the order of the frequency by ℓ: $\omega_n \to \omega_\ell$.

In the following the term *quasi normal mode* will refer to only their frequencies ω rather than to their amplitudes A.

2 Methods

2.1 Time Evolution

2.1.1 Naive Approach

This method which straightforward uses the plain Schwarzschild metric with Eddington-Finkelstein coordinates will be later referred to as *naive* method.

To solve equation (1) or (2) respectively, $\Phi(t, r, \vartheta, \varphi)$ is written as a composition of a radial part $\phi_{\ell m}(t, r)$ and spherical harmonics $Y_{\ell m}(\vartheta, \varphi)$:

$$\Phi(t, r, \vartheta, \varphi) = \sum_{\ell=0}^{\infty} \sum_{m=-\ell}^{\ell} Y_{\ell m}(\vartheta, \varphi)\phi_{\ell m}(t, r) \tag{21}$$

By inserting this into equation (1) one gets due to the differential property of the spherical harmonics

$$\Box\Phi = \sum_{\ell,m} Y_{\ell m}(\vartheta, \varphi)\ \ (\Box\phi_{\ell m}(t, r)) + \sum_{\ell,m} \phi_{\ell m}(t, r)\ \ (\Box Y_{\ell m}(\vartheta, \varphi)) \tag{22}$$

$$= \sum_{\ell,m} Y_{\ell m}(\vartheta, \varphi)\ \Box_{tr}\phi_{\ell m}(t, r) + \sum_{\ell,m} \phi_{\ell m}(t, r) \left(-\frac{\ell(\ell+1)}{r^2}\right) Y_{\ell m}(\vartheta, \varphi) \tag{23}$$

$$= \sum_{\ell,m} \left(\Box_{tr} - \frac{\ell(\ell+1)}{r^2}\right) \phi_{\ell m}(t, r)Y_{\ell m}(\vartheta, \varphi). \tag{24}$$

$\Box_{t,r}$ is the wave operator which only differentiates with respect to t and r. The sum $\sum_{\ell,m}$ is the same as in equation (21) written in a compact form. Because $\{Y_{\ell m}(\vartheta)\}_{\ell m}$ forms an orthonormal base, we can express $\Phi(t, r, \vartheta, \varphi)$ as a projection of $\phi_\ell(t, r)$ on the spherical harmonics which leads to

$$\left(\Box_{tr} - \frac{\ell(\ell+1)}{r^2}\right) \phi_{\ell m}(t, r) = 0 \tag{25}$$

for each ℓ. This generalises due to its linearity, via equation (2) to

$$\frac{1}{\sqrt{g}}\partial_\mu \left(\sqrt{g}\ g^{\mu\nu}\partial_\nu\phi_{\ell m}\right) - \frac{\ell(\ell+1)}{r^2}\phi_{\ell m} = 0\ , \tag{26}$$

where the indices μ, ν only cover t, r. The index m can be dropped because due to the spherical symmetry of the Schwarzschild solution Φ does not depend on φ and $\phi_{\ell m}$ not on m.

If equation (26) is evaluated with the Schwarzschild metric in Eddington-Finkelstein coordinates Eq. (10), we get for each ℓ a differential equation for $\phi_\ell(t_*, r)$:

$$\begin{aligned}\partial_{t_*}^2 \phi_\ell = \Bigg[& \frac{1 - \frac{2m}{r}}{1 + \frac{2m}{r}} \partial_r^2 + \frac{2(r-m)}{r(r+2m)} \partial_r + \frac{2m}{r(r+2m)} \partial_{t_*} + \\ & + \frac{4m}{r+2m} \partial_{t_*} \partial_r - \frac{\ell(\ell+1)}{r^2} \Bigg] \phi_\ell \end{aligned} \tag{27}$$

A solution to equation (27) can be obtained by numerically evolving some initial data[4] $\phi(0, r)$, $\partial_{t_*} \phi(t_*, r)|_{t_*=0}$. To perform this time evolution, the order of the differential equation is reduced, it is split into two coupled differential equations containing only first order time derivatives via the substitution $\psi_\ell(t_*, r) = \partial_{t_*} \phi_\ell(t_*, r)$:

$$\partial_{t_*} \phi_\ell = \psi_\ell \ , \tag{28}$$

$$\begin{aligned}\partial_{t_*} \psi_\ell = & \frac{1 - \frac{2m}{r}}{1 + \frac{2m}{r}} \partial_r^2 \phi_\ell + \frac{2(r-m)}{r(r+2m)} \partial_r \phi_\ell + \frac{2m}{r(r+2m)} \psi_\ell + \\ & + \frac{4m}{r+2m} \partial_r \psi_\ell - \frac{\ell(\ell+1)}{r^2} \phi_\ell \end{aligned} \tag{29}$$

This system of equations can be solved with time evolution techniques for differential equations. We use a second order Runge-Kutta method [12] where both equations (28) and (29) are integrated in parallel. As initial data, an ingoing or an outgoing Gaussian pulse corresponding to

$$\phi(t_*, r) = \frac{1}{\sqrt{2\pi\sigma^2}} e^{\frac{-(r - r_c \pm c t_*)^2}{2\sigma^2}} \ , \quad + \text{ for outgoing , } - \text{ for ingoing} \tag{30}$$

is used. In equation (30) σ is the standard deviation of the Gaussian pulse and r_c is the position of its maximum.

The simulation is performed on a grid reaching spatially from the Schwarzschild radius at $r = 2m$ to a boundary at $r = R$ large enough so that effects from the boundary can not reach the region close to the black hole in the simulated time. On the first grid point, one-sided difference schemes are used to be independent of information inside the Schwarzschild radius, which would be physically incorrect. The used finite difference schemes are listed in the Appendix in section A.1. On the grid point at R the function is kept constant at $\phi(t_*, R) = 0$ as the Dirichlet boundary condition. The evolution of such a simulation is shown in figures 3 and 4.

The field $\phi_\ell(t_*, r)$ obtained by the time evolution is inspected by fixing r at some r_{fix} and fitting $\phi_\ell(t_*, r_{\text{fix}})$ with equation (19) to obtain the quasi normal modes $\omega_{\ell,\text{re}}$ and $\omega_{\ell,\text{im}}$. Such a fit is shown in figure 5.

The procedure described above is done for each ℓ, we are interested in, to receive the set $\{\omega_\ell\}$.

[4] The initial data is the same for all ℓ-s. Therefore $\phi(0, r)$ is not indicated with a specific ℓ.

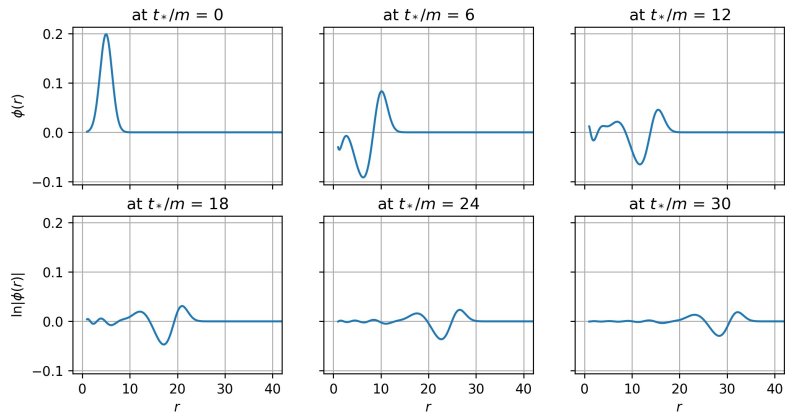

Figure 3: Evolution of the initial data (30) with $r_c = 5$, $\sigma = 0.8$ simulated at a discretisation $\Delta t_* = 0.0028$, $\Delta r = 0.075$ at different times computed with the naive method. From the time $t_*/m = 18$ the quasi normal ringdown can be observed.

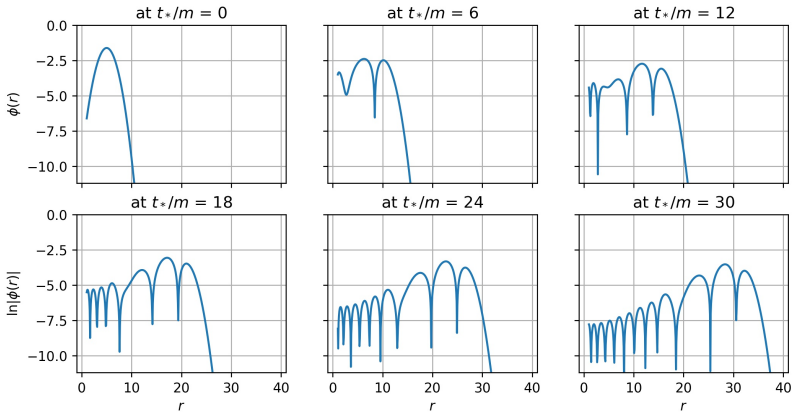

Figure 4: Evolution of the initial data shown as $\ln|\phi(r)|$ with the same parameters as in figure 3. As in figure 2 and many of the following diagrams, a logarithmic representation is displayed because the exponential decay in time of a QNM otherwise hides a lot of the context.

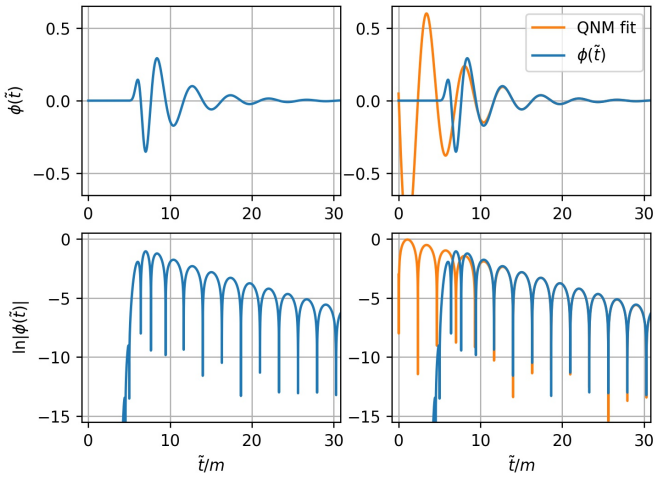

Figure 5: Fit of $\phi_5(r)$ as a quasi normal mode Eq. (19), simulated with the same parameters as in figure 3. The quasi normal frequency reads out as $\omega_5 = 2.12 + 0.19i$.

2.1.2 CMC Foliation

This method will later be referred to as the *CMC* method, to compare it and its results with other methods.

Written with the substitutions lapse α, the shift β and the spatial metric function γ

$$\alpha = \frac{\tilde{P}(\tilde{r})}{\tilde{r}^2} \ , \quad \beta = \left(\frac{C\Omega^3}{\tilde{r}^3} - \frac{K\tilde{r}}{3} \right) \ , \quad \gamma = \frac{1}{\alpha} \tag{31}$$

the metric from equation (15) can be expressed as

$$\mathrm{d}s^2 = \left(\gamma^2\beta^2 - \alpha^2\right) \ \mathrm{d}\tilde{t}^2 + 2\gamma^2\beta \ \mathrm{d}\tilde{t} \ \mathrm{d}\tilde{r} + \gamma^2 \ \mathrm{d}\tilde{r}^2 + \tilde{r}^2 \ \mathrm{d}\hat{\sigma}^2. \tag{32}$$

With this it is possible to obtain a system of equations for $\phi_\ell(\tilde{t}, \tilde{r})$,

$$\psi_\ell(\tilde{t}, \tilde{r}) := \partial_{\tilde{t}}\phi_\ell(\tilde{t}, \tilde{r}) \quad \text{and} \quad \rho_\ell(\tilde{t}, \tilde{r}) := \frac{\gamma}{\alpha}\left(\partial_{\tilde{t}}\phi_\ell(\tilde{t}, \tilde{r}) - \beta\partial_{\tilde{r}}\psi_\ell(\tilde{t}, \tilde{r})\right) \tag{33}$$

as in [13]:

$$\begin{aligned} \partial_{\tilde{t}}\phi_\ell &= \frac{\alpha}{\gamma}\rho_\ell + \beta\psi_\ell \ , \quad \partial_{\tilde{t}}\psi_\ell = \partial_{\tilde{r}}\left(\frac{\alpha}{\gamma}\rho_\ell + \beta\psi_\ell\right) \ , \\ \partial_{\tilde{t}}\rho_\ell &= \frac{1}{r^2}\partial_{\tilde{r}}\left(\tilde{r}^2\left(\frac{\alpha}{\gamma}\rho_\ell + \beta\rho_\ell\right)\right) - \left(\frac{1}{6}\tilde{R}\phi_\ell + \frac{\ell(\ell+1)}{\tilde{r}^2}\phi_\ell\right) \end{aligned} \tag{34}$$

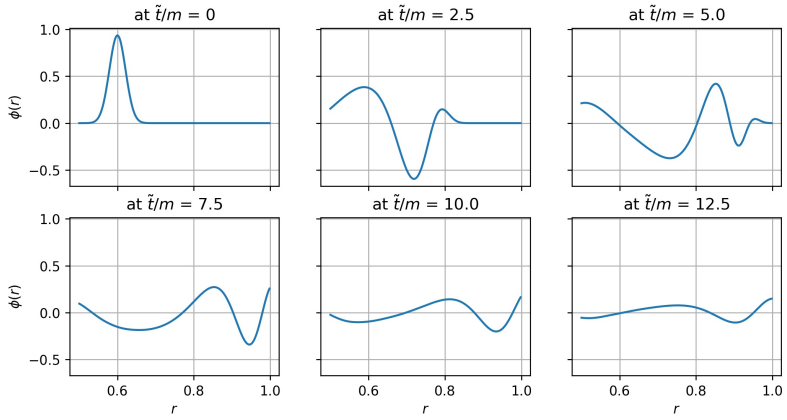

Figure 6: Evolution of the initial data (35) with $r_c = 0.6$, $\sigma = 0.03$ simulated at a discretisation $\Delta\tilde{t} = 0.001$, $\Delta\tilde{r} = 0.002$ computed with the CMC method.

Here $\phi_\ell(\tilde{t}, \tilde{r})$ is used rather than $\tilde{\phi}_\ell(\tilde{t}, \tilde{r})$ even though the latter would be formally rigorous, to reduce complexity in notation. The space time in which the function ϕ_ℓ is defined is concluded by its arguments.

This system can also be solved with time evolution techniques to evolve initial data. In [13] initial data in the form of

$$\begin{aligned} &\phi(0,\tilde{r}) = a\ e^{-(\tilde{r}-r_c)^2/\sigma^2}\ , \quad \psi(0,\tilde{r}) = -\frac{2(\tilde{r}-r_c)}{\sigma^2}\ \phi(0,\tilde{r})\ , \\ &\rho(0,\tilde{r}) = -\psi(0,\tilde{r}) - \frac{\phi(0,\tilde{r})}{\tilde{r}}\left(1 - \frac{\beta\gamma}{\alpha}\right). \end{aligned} \tag{35}$$

is proposed. Here, as in equation (30), σ is the standard deviation of the Gaussian pulse and r_c is the position of its maximum. Notice that $\psi_\ell(0,\tilde{r})$ and $\rho_\ell(0,\tilde{r})$ are obtained by plugging the pulse $\phi_\ell(\tilde{t},\tilde{r}) = a\ e^{-(\tilde{r}-r_c+\tilde{t})^2/\sigma^2}$ into the definitions in equation (33) and setting $\tilde{t} = 0$. So $\phi_\ell(\tilde{t},\tilde{r})$ takes a similar form as the initial data used in the first approach when the outgoing sign in equation (30) is chosen.

One convenient point about the foliation is that with $\tilde{r} \in [0.5, 1]$ one can observe the whole region between the event horizon and *null infinity* and does not have to consider boundary effects induced by a truncation of the simulation at some distance R, cf. figure 1.

The system from equation (34) is evolved using a second order Runge-Kutta method on a second order discretization in space. At the event horizon and at *null infinity* one-sided difference schemes are used. The simulation is performed on a mesh with the conditions mentioned above and the initial data from equation (35). The first oscillations of such a simulation are shown in the figures 6 and 7.

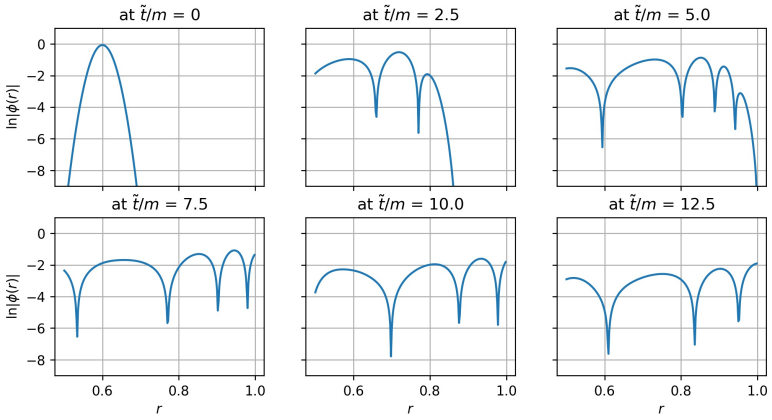

Figure 7: Evolution of the initial data, computed with the same parameters as in figure 6 shown as $\ln|\phi(\tilde{r})|$.

As in section 2.1.1 the solutions $\phi_\ell(\tilde{t}, \tilde{r})$ are analysed by fitting them at r_{fix} with equation (19) to obtain $\{\omega_\ell\}$.

2.1.3 Artificial Dissipation

Both time evolution methods presented above are implemented with the use of artificial dissipation. It works like a low-pass filter which smooths out ϕ_ℓ in the radial direction. This is done to prevent noise from growing and becoming unsteady points in the solution. Physically it is not a problem to filter out these parts of the solution, since the higher frequencies propagate less under the impact of the wave equation, see [4].

The artificial dissipation for the second order scheme is applied by subtracting the term

$$\frac{\epsilon}{16}\left(\phi^{i-1}_{j+2} - 4\phi^{i-1}_{j+1} + 6\phi^{i-1}_{j} - 4\phi^{i-1}_{j-1} + \phi^{i-1}_{j-2}\right) \ , \tag{36}$$

where $\phi^i_j = \phi(t_i, x_j)$ is the discretised field ϕ, from the right hand side of the differential equations for $\partial_t\phi$ (Eq. (28) and (34)), where $0 < \epsilon < 1$ is an adjustable parameter used to control the impact of the artificial dissipation.

2.2 Semi-Analyical Methods

2.2.1 Perturbation Theory

Another approach to QNM uses perturbation theory [8]. There the view is on a perturbed black hole described by a perturbed metric

$$g_{\mu\nu} = g^0_{\mu\nu} + \delta g_{\mu\nu} \tag{37}$$

where $g^0_{\mu\nu}$ is the non-perturbed metric, like for example the Schwarzschild metric, and $\delta g_{\mu\nu}$ is a perturbation with $|g^0_{\mu\nu}| \gg |\delta g_{\mu\nu}|$. The perturbation can come from the excitation of the black hole by some signal like gravitational waves (its interaction with macroscopic objects reacting gravitationally).

As shown in [3], [10] and [8] such a problem can be transformed to the problem of solving a Schrödinger-like differential equation

$$-\frac{\mathrm{d}^2\psi_\ell(t,r_*)}{\mathrm{d}r^2} + V(r_*,\omega)\psi_\ell(t,r_*) = \omega^2\psi_\ell(t,r_*) \tag{38}$$

where ψ_ℓ is, like ϕ_ℓ in previous sections, the radial part of a decomposed function $\Psi(t,r_*,\vartheta,\varphi) = \sum_{\ell,m} Y_{\ell m}(\vartheta,\varphi)\psi_\ell(t,r_*)$ and r_* again denotes the tortoise coordinate (8). The potential $V(r_*,\omega)$ is

$$V(r_*,\omega) = \left(1-\frac{2m}{r_*}\right)\left(\frac{\ell(\ell+1)}{r_*^2} + \frac{2m\left(1-s^2\right)}{r_*^3}\right) \tag{39}$$

as it is presented in [8]. For $s = 0$, the equation gives the effective potential of a scalar field which is the kind of field we are looking at in this thesis. With $s = 1$ it gives the potential for a Maxwell field and $s = 2$ gives the potential of the gravitational perturbations of the axial type.

To solve equation (38) for a unique solution, boundary conditions for ψ_ℓ are needed. In [8] and [10] the same conditions are described:

$$\begin{aligned} \psi_\ell \text{ is a pure ingoing wave for } r_* \to -\infty \\ \psi_\ell \text{ is a pure outgoing wave for } r_* \to +\infty \end{aligned} \tag{40}$$

By solving equation (38) for $\psi_\ell(t,r)$ one obtains the quasi normal modes ω_ℓ for different ℓ-s.

2.2.2 Shooting Method

As shown in [3] the differential equation (38) can be reduced to the so-called Riccati equation

$$i\frac{\mathrm{d}\theta_\ell}{\mathrm{d}r_*} + \omega_\ell^2 - \theta_\ell^2 + V(r_*,\omega) = 0 \tag{41}$$

by using the substitution[5]

$$\psi_\ell = \exp\left(i\int^{r_*}\theta_\ell \, \mathrm{d}r_*\right). \tag{42}$$

The boundary conditions from equation (40) translate as

$$\begin{aligned} \psi_\ell \to +\omega_\ell \text{ for } r_* \to -\infty \\ \psi_\ell \to -\omega_\ell \text{ for } r_* \to +\infty. \end{aligned} \tag{43}$$

[5]The function θ_ℓ shall not be confused with ϑ which describes the horizontal angle in the spherical coordinate system.

In order to obtain the quasi normal modes, the Riccati equation (41) needs to be solved for θ_ℓ. In [3] it is suggested to do so by "shooting" the two asymptotic solutions noted above in equation (43) from $r_* \ll -1$ and $r_* \gg 1$ at some common intermediate point r_c. This point is chosen usually to be the peak of the potential $V(r_*, \omega)$.

In summary the shooting procedure is the following: One starts with a function $\psi_{\leftarrow} \propto e^{i\omega r_*}$ with some fixed complex ω and integrate it with equation (41) from some r_* big enough that we can assume the boundary conditions to hold backwards to r_c. Then we take a function $\psi_{\rightarrow} \propto e^{-i\omega r_*}$ with the same ω and integrate it from somewhere close enough to the horizon forward to r_*. At the common point the Wronskian of the two solutions must vanish if the value for ω belongs to a quasi normal mode. This condition then gives a equation for the quasi normal modes ω.

This method seems fairly straightforward but it is mentioned in [3] as being "beset" with numerical instabilities. For large positive r_* the solution ψ with the asymptotic behaviour $\psi_{\leftarrow} \propto e^{i\omega r_*}$ gets mixed with solutions $\propto e^{-i\omega r_*}$ which are exponentially small at this large r_* but grow bigger by integrating backwards and at the common point they will be noticeable. That means the solution does not longer fulfill the specified conditions. The same applies vice versa for the solution ψ with $\psi_{\rightarrow} \propto e^{-i\omega r_*}$ at the horizon.

Given the challenges mentioned above and the availability of other semi analytical methods the shooting method is not followed up any further.

2.2.3 Method of Continued Fractions

The results obtained by the previously discussed shooting method are insufficient, that is why the method of continued fractions is used. This method will from now on be referred to as the *analytic* or the *semi analytic* method.

Equation (38) can be solved by a function which satisfies the boundary conditions so that it is a purely in-going wave at the event horizon and a purely out-going wave at spatial infinity. This function can be written in the form

$$\psi_\ell(t, r_*) = (1 - r_*)^{-i\omega} r_*^{2i\omega} e^{i\omega(r_* - 1)} \sum_{n=0}^{\infty} a_n \left(\frac{r_* - 1}{r_*} \right)^n \tag{44}$$

as it is done in [10] where it is referred to be from [1]. The sequence of coefficients $\{a_n\}_{n \in \mathbb{N}}$ is determined by a repetitive formula with the starting conditions $a_0 = 1$ and $\alpha_{-1} = 0$:

$$\alpha_n a_{n+1} + \beta_n a_n + \gamma_n a_{n-1} = 0 \tag{45}$$

The coefficients[6] α_n, β_n and γ_n are defined as functions of n and ω:

$$\begin{aligned}\alpha_n &= n^2 + (2(-i\omega) + 2)n + 2(-i\omega) + 1 \\ \beta_n &= -\left(2n^2 + (2 - 8i\omega)n - 8\omega^2 - 4i\omega + \ell(\ell+1) + \left(1 - s^2\right)\right) \\ \gamma_n &= n^2 - 4ni\omega - 4\omega^2 + \left(1 - s^2\right) - 1\end{aligned} \tag{46}$$

The s plays the same role as in the potential in equation (39): For $s = 0$, the equation gives the effective potential of a scalar field, with $s = 1$ it gives the potential for a Maxwell field and $s = 2$ gives the potential of the gravitational perturbations of the axial type. Plugging those coefficients into equation (45) and computing the ratio a_{n+1}/a_n gives the infinite continued fraction[7]

$$\begin{aligned}\frac{a_{n+1}}{a_n} &= \cfrac{-\gamma_{n+1}}{\beta_{n+1} - \cfrac{\alpha_{n+1}\gamma_{n+2}}{\beta_{n+2} - \cfrac{\alpha_{n+2}\gamma_{n+3}}{\beta_{n+3} - \cdots}}} \\ &= \cfrac{-\gamma_{n+1}}{\beta_{n+1} + \mathrm{K}_{m=n+1}^{\infty} \cfrac{-\alpha_m\gamma_{m+1}}{\beta_{m+1}}}.\end{aligned} \tag{47}$$

This gives two conditions for the ratio a_1/a_0, one from the starting condition of the sequence $\{a_n\}_{n\in\mathbb{N}}$ and the other one from equation (47):

$$\frac{a_1}{a_0} = -\frac{\beta_0}{\alpha_0} \tag{48}$$

$$\frac{a_1}{a_0} = \cfrac{-\gamma_1}{\beta_1 + \mathrm{K}_{m=1}^{\infty} \cfrac{-\alpha_m\gamma_{m+1}}{\beta_{m+1}}} \tag{49}$$

By setting those equations equal to each other, an implicit characteristic equation for the quasi normal modes ω can be obtained:

$$\begin{aligned}0 &= \beta_0 - \cfrac{\alpha_0\gamma_1}{\beta_1 - \cfrac{\alpha_1\gamma_2}{\beta_2 - \cfrac{\alpha_2\gamma_3}{\beta_3 - \cdots}}} \\ &= \beta_0 + \mathrm{K}_{m=0}^{\infty} \frac{-\alpha_m\gamma_{m+1}}{\beta_{m+1}}\end{aligned} \tag{50}$$

Since α_n, β_n and γ_n are simple polynomial functions of the quasi normal frequencies ω_ℓ, equation (50) can be taken as their defining equation. I order to find the quasi normal modes, just the roots of equation (50) with respect to ω_ℓ have to be found.

After truncation of the infinite fraction at a high enough m, the roots can be found with e.g. Newton's method and the use of a computer algebra system.

[6] Note that these symbols represent something else than the α, β and γ defined in section 1.2.2 and used in section 2.1.2. The symbols defined here are only valid for this section.

[7] In equation (47) and the following equations Gauss' notation of continued fractions K is used. It has a syntax similar to that of a sum Σ or a product Π. For example:

$$\mathrm{K}_{i=0}^{2} \frac{a_i}{b_i} = \cfrac{a_0}{b_0 + \cfrac{a_1}{b_1 + \cfrac{a_2}{b_2}}}$$

As a guess for the first mode ω_0 one can use a confirmed value from relevant literature. The value of ω_ℓ is a sufficient guess for $\omega_{\ell+1}$ only for small ℓ-s.

The first few ω_ℓ-s can be computed by predicting them with the previous $\omega_{\ell-1}$. Those values are then fitted linearly for the real parts and in the form of $\omega_{\ell,\mathrm{im}} = a\ell^{-\kappa} + b$. With the fitted parameters the quasi normal frequencies are predicted and then calculated with a high precision by the root finding algorithm.

3 Results

The results of the fitted first ten quasi normal modes is displayed in table 1. The same values are plotted in figure 8. In figure 9 only the more accurate results of the CMC and the analytical method are shown. In both figures they are compared with the estimated values computed with equation (20) which are valid for large ℓ-s.

Table 1: Results of ω_ℓ with at least six significant digits.

ℓ	CMC	naive	analytic
0	$0.177\,226 + 0.197\,361i$	$0.188\,077 + 0.197\,641i$	$0.220\,910 + 0.209\,791i$
1	$0.581\,777 + 0.193\,719i$	$0.739\,905 + 0.207\,340i$	$0.585\,872 + 0.195\,320i$
2	$0.967\,352 + 0.194\,311i$	$1.247\,566 + 0.203\,947i$	$0.967\,288 + 0.193\,518i$
3	$1.350\,705 + 0.193\,732i$	$1.757\,848 + 0.199\,872i$	$1.350\,732 + 0.192\,999i$
4	$1.734\,836 + 0.193\,440i$	$2.274\,930 + 0.194\,929i$	$1.734\,831 + 0.192\,783i$
5	$2.119\,238 + 0.193\,233i$	$2.804\,279 + 0.187\,237i$	$2.119\,224 + 0.192\,674i$
6	$2.503\,789 + 0.193\,066i$	$3.347\,386 + 0.184\,843i$	$2.503\,773 + 0.192\,610i$
7	$2.888\,437 + 0.192\,918i$	$3.908\,837 + 0.188\,377i$	$2.888\,416 + 0.192\,570i$
8	$3.273\,151 + 0.192\,777i$	$4.489\,487 + 0.202\,723i$	$3.273\,120 + 0.192\,544i$
9	$3.657\,910 + 0.192\,642i$	$5.093\,147 + 0.229\,973i$	$3.657\,866 + 0.192\,525i$

All displayed results refer to natural units $c = G = 1$ and a black hole with mass $M = 1/2$, thus $m = 1/2$. The details for the procedures are the following:

- naive method: $\Delta r = 0.075$, $\Delta t = 0.0028$, $R = 120$, $T = 60$; which leads to about $34 \cdot 10^6$ grid points. The initial condition is used in the form of an outgoing wave.
- CMC method: $\Delta r = 0.002$, $\Delta t = 0.001$, $T = 100$; which leads to about $25 \cdot 10^6$ grid points.
- analytic method: Truncation of the continued fraction after 900 nesting levels for the computation of the guessing values for the root finding algorithm, then truncation after a nesting depth of 1 500.

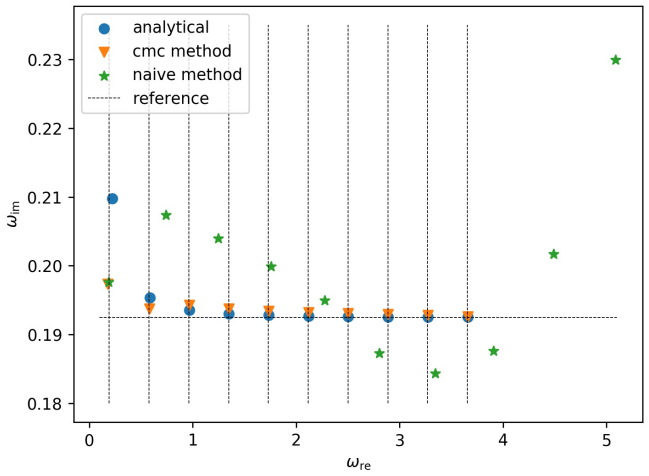

Figure 8: Comparison of the results for different methods. The dashed lines are real (vertical) and complex (horizontal) values for quasi normal modes ω_ℓ computed with the estimator from equation (20), for $n = 0$ and $\ell = 0, \ldots, 9$.

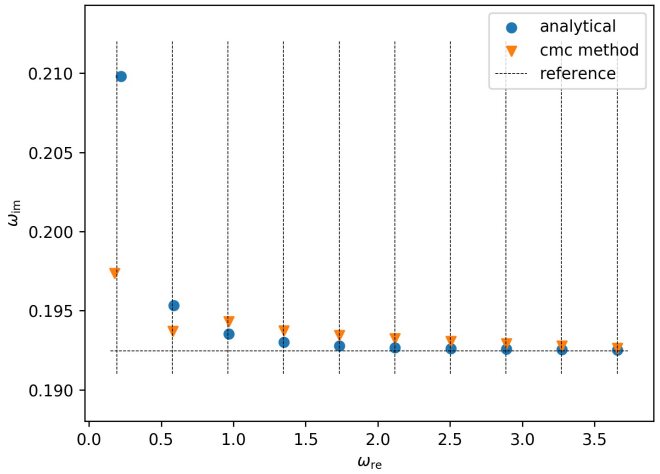

Figure 9: Comparison of the results from the CMC method and the semi analytical method of continued fractions. The dashed lines are as previously values for quasi normal modes ω_ℓ, for $n = 0$ and $\ell = 0, \ldots, 9$.

4 Discussion

4.1 Methods

Apart from the greater physical consistency mentioned in section 2.1.2 the CMC method has two other advantages over the naive method.

Firstly, there is no need to rescale the spatial range when changing the simulation time. The results of the naive method are obtained by solving the differential equations on a grid, where the spatial range is $2c$-times wider than the time range.[8]. This is done to prevent boundary effects from the Dirichlet condition at $r = R$ from having any impact on a signal starting at $t = 0$, $r = 2m$. The grid $T \times R = T \times 2c \cdot T = 2c \cdot T^2$ scales quadratically with respect to T which makes the simulation scale at least like $\mathcal{O}(T^2 R)$.

The CMC method instead – due to its foliated grid reaching *null infinity* – has a fixed spatial grid by design. Artefacts caused by truncation are not an issue with this method. In that sense the computational complexity of the CMC method scales like $\mathcal{O}(TR)$.

The second advantage of the CMC method is the possibility to measure the quasi normal frequency as far away from the source as physically possible – at *null infinity*. In contrast with the CMC method a limitation is the size of the simulation grid, as useful results can only be obtained in a region with $r_{\text{fix}} < R/2$.

4.2 Results

It is found that there is a clearly visible difference of accuracy between the values obtained with the naive method and the ones from the CMC and semi analytic methods. This can be seen in figure 8. The first deviate from the reference values both in their real and imaginary part. The frequency ω_{re} linearly, with a rate about 1.4 times too fast. The damping ω_{im} does not appear to aim for the proposed value for a growing ℓ at all.

The values obtained with the CMC and the semi analytical method on the other hand are behaving in a way which confirms the assumption stated in equation (20). The frequency ω_{re} grows consistently with the prediction in a linear way for growing ℓ. The damping ω_{im} asymptotically approaches the reference value, whereby the semi analytically obtained values converge faster.

The deviation in the real part of the quasi normal frequencies ω_0 obtained by the naive and the CMC method can to some extent be explained with the help of figure 10. There $\phi_0(\tilde{t}, \tilde{r})$ is shown at $\tilde{r} = r_{\text{fix}} = \textit{null infinity}$ as a function of time. It can be seen that the quasi normal ringdown does last for less than half a period, which limits the information available for the fitting drastically. Therefore the accuracy of the quasi normal frequency can be compromised.

[8] In terms of section 2.1.1: $R = 2c \cdot T$.

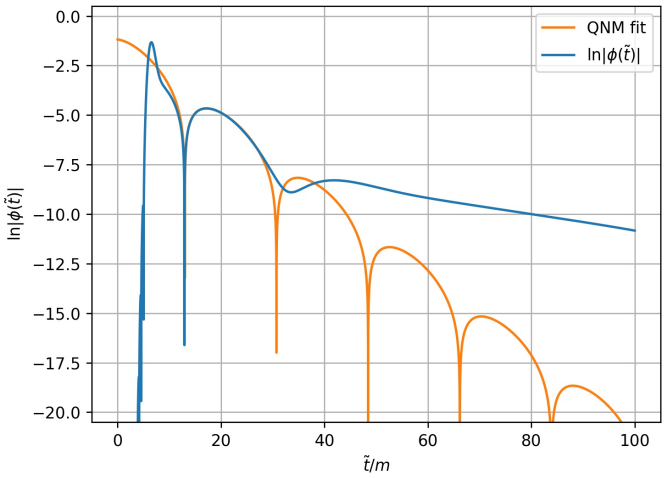

Figure 10: QNM Fit for the CMC computed mode with $\ell = 0$. $\ln|\phi(\tilde{t})|$ is shown at $\tilde{r} =$ *null infinity*.

5 Outlook

Accuracy can be increased by improving the fitting of the results of the naive and the CMC method. This can be done by not only fitting one quasi normal mode in a timescale, where the faster decaying higher modes have already vanished, but fitting a superposition of the first two or three quasi normal modes for the same ℓ over a wider timescale. E.g:

$$\chi_\ell(t) = \sum_{n=0}^{3} A_n \cos(\omega_{n,\mathrm{re}} t + \delta_n)\ e^{-\omega_{n,\mathrm{im}} t + \delta_n} \tag{51}$$

Another point would be to add a nonlinear inhomogeneity to the wave equation, for example instead of $\Box\Phi = 0$, solving

$$\Box\Phi = \Phi^3. \tag{52}$$

This could, for small initial data mimic non-linearities of the Einstein equations. But due to its non-linearity such a equation may need a different approach.

A Appendix

A.1 Finite Difference Schemes

Below are listed the finite difference schemes which are used in the numerical time evolution simulations, as they appear for example in [5].

- Central difference scheme second order for first order derivative:

$$\left.\frac{\partial u}{\partial x}\right|_{x_i} = \frac{u_{i+1} - u_{i-1}}{2\Delta x} - \frac{\Delta x^2}{6} \left.\frac{\partial^3 u}{\partial x^3}\right|_{x_i} + \dots \tag{53}$$

- Left/Right-sided difference scheme second order for first order derivative:

$$\left.\frac{\partial u}{\partial x}\right|_{x_i} = \frac{\pm 3u_i \mp 4u_{i\mp 1} \pm u_{i\mp 2}}{2\Delta x} + \frac{\Delta x^2}{3} \left.\frac{\partial^3 u}{\partial x^3}\right|_{x_i} + \dots \tag{54}$$

  Choose the upper sign for the left-sided and the lower sign for the right-sided scheme.

- Central difference scheme second order for second order derivative:

$$\left.\frac{\partial^2 u}{\partial x^2}\right|_{x_i} = \frac{u_{i+1} - 2u_i - u_{i-1}}{\Delta x^2} - \frac{\Delta x^2}{12} \left.\frac{\partial^4 u}{\partial x^4}\right|_{x_i} + \dots \tag{55}$$

- Left/Right-sided difference scheme second order for second order derivative:

$$\left.\frac{\partial^2 u}{\partial x^2}\right|_{x_i} = \frac{2u_i - 5u_{i\mp 1} + 4u_{i\mp 2} - u_{i\mp 3}}{\Delta x^2} \mp \frac{11\Delta x^2}{12} \left.\frac{\partial^4 u}{\partial x^4}\right|_{x_i} + \dots \tag{56}$$

  Choose the upper sign for the left-sided and the lower sign for the right-sided scheme.

A.2 Code

The simulations for the naive method, the CMC method and some utility functions to analyse and plot the data are programmed in Python. The developed code can be examined at `github.com/wolfgruber/quasi_normal_modes`.

A.3 Convergence

In figures 11 and 12 the convergence factor Q, see [4], is plotted as a function of time:

$$Q(t) = \frac{\|\phi^{\Delta r}(t,r) - \phi^{2\Delta r}(t,r)\|_r}{\|\phi^{2\Delta r}(t,r) - \phi^{4\Delta r}(t,r)\|_r} \sim 2^p \tag{57}$$

$\phi^{\Delta r}(t,r)$ refers the field $\phi(t,r)$ computed with a specific spatial grid size Δr and the norm $\|\dots\|_r$ is the Euclidean norm for fixed t. The subtractions are of course only performed on those grid points of $\phi^{n\Delta r}(t,r)$ and $\phi^{2n\Delta r}(t,r)$ which match. The quantity Q is defined in such a way that in the limit $\Delta r \to 0$ it converges to 2^p, where p is the order of the used algorithm, for details see [4].

The convergence factors in figures 11 and 12 indicate that the used algorithms have at least a 2nd order convergence. The CMC method seems to converge with 3rd order, which can depend on the specific parameters used[13].

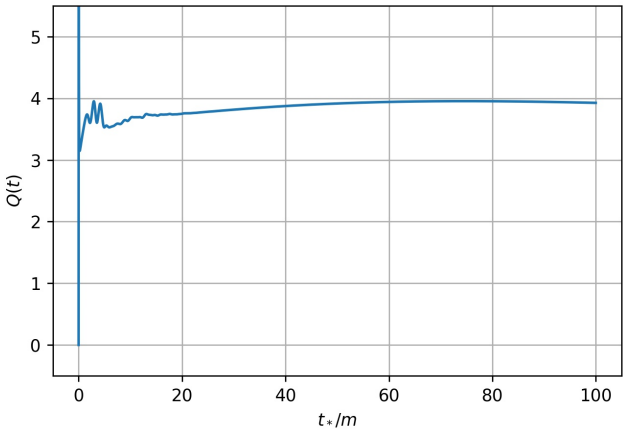

Figure 11: Convergence for the naive method, computed with $\Delta t_* = 0.016$, $\Delta r = 0.4$.

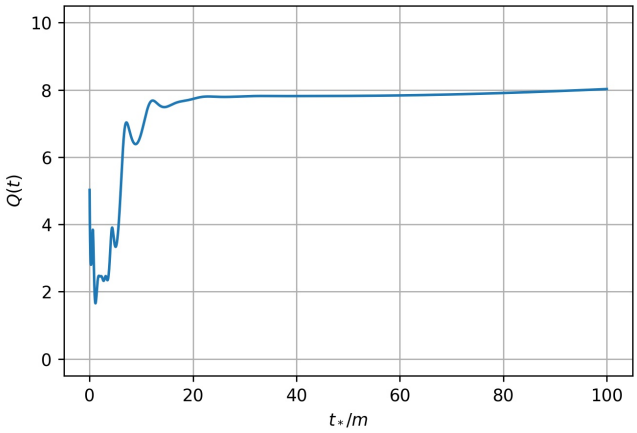

Figure 12: Convergence for the CMC method, computed with $\Delta \tilde{t} = 0.016$, $\Delta \tilde{r} = 0.02$.

References

[1] W. G. Baber and H. R. Hassé. 'The Two Centre Problem in Wave Mechanics'. In: *Mathematical Proceedings of the Cambridge Philosophical Society* 31.4 (1935), pp. 564–581. DOI: 10.1017/S0305004100013566.

[2] Matthias Bartelmann et al. 'Schwingungen'. In: *Theoretische Physik*. Berlin, Heidelberg: Springer Berlin Heidelberg, 2015, pp. 211–242. ISBN: 978-3-642-54618-1. DOI: 10.1007/978-3-642-54618-1_6. URL: https://doi.org/10.1007/978-3-642-54618-1_6.

[3] Subrahmanyan Chandrasekhar and S. Detweiler. 'The quasi-normal modes of the Schwarzschild black hole'. In: (Aug. 1975). URL: https://doi.org/10.1098/rspa.1975.0112.

[4] Matthew W. Choptuik. *Contents 1 Basic Finite Difference Techniques for Time Dependent PDEs 2*. 2006. URL: https://core.ac.uk/download/pdf/22880005.pdf.

[5] Ardeshir Hanifi. *Finite Difference Schemes*. URL: https://www.mech.kth.se/~ardeshir/courses/literature/fd.pdf.

[6] Peter Hübner. 'Method for calculating the global structure of (singular) spacetimes'. In: *Phys. Rev. D* 53 (2 Jan. 1996), pp. 701–721. DOI: 10.1103/PhysRevD.53.701. URL: https://link.aps.org/doi/10.1103/PhysRevD.53.701.

[7] Kostas D. Kokkotas and Bernd G. Schmidt. 'Quasi-Normal Modes of Stars and Black Holes'. In: *Living Reviews in Relativity* 2.1 (Sept. 1999). ISSN: 1433-8351. DOI: 10.12942/lrr-1999-2. URL: http://dx.doi.org/10.12942/lrr-1999-2.

[8] R. A. Konoplya and Alexander Zhidenko. 'Quasinormal modes of black holes: From astrophysics to string theory'. In: *Reviews of Modern Physics* 83.3 (July 2011), pp. 793–836. DOI: 10.1103/RevModPhys.83.793. arXiv: 1102.4014 [gr-qc].

[9] Lev Davidovič Landau and Evgenij M. Lifšic. *The classical theory of fields*. eng. 3. print.. Addison-Wesley series in advanced physics. Reading, Mass. [u.a.]: Addison-Wesley [u.a.], 1961. Chap. 10.

[10] E. W. Leaver. 'An Analytic Representation for the Quasi-Normal Modes of Kerr Black Holes'. In: *Proceedings of the Royal Society of London Series A* 402.1823 (Dec. 1985), pp. 285–298. DOI: 10.1098/rspa.1985.0119.

[11] Charles W Misner. *Gravitation*. eng. First Princeton University Press edition. Princeton Oxford: Princeton University Press, 2017. ISBN: 9780691177793.

[12] Ashok Kumar Singh. *Numerical methods for ordinary differential equations with programs*. eng. Oxford, U.K. : Alpha Science International Ltd., 2018. ISBN: 9781783324415.

[13] Anıl Zenginoğlu. 'A hyperboloidal study of tail decay rates for scalar and Yang–Mills fields'. In: *Classical and Quantum Gravity* 25.17 (Aug. 2008), p. 175013. DOI: 10.1088/0264-9381/25/17/175013. URL: https://doi.org/10.1088%2F0264-9381%2F25%2F17%2F175013.